c-Abl regulates YAP^{Y357} phosphorylation to activate endothelial atherogenic responses to disturbed flow

Bochuan Li, Jinlong He, Huizhen Lv, Yajin Liu, Xue Lv, Chenghu Zhang, Yi Zhu, and Ding Ai

Tianjin Key Laboratory of Metabolic Diseases; Key Laboratory of Immune Microenvironment and Disease (Ministry of Education); Collaborative Innovation Center of Tianjin for Medical Epigenetics and Department of Physiology and Pathophysiology, Tianjin Medical University, Tianjin, China.

Local flow patterns determine the uneven distribution of atherosclerotic lesions. This research aims to elucidate the mechanism of regulation of nuclear translocation of Yes-associated protein (YAP) under oscillatory shear stress (OSS) in the atheroprone phenotype of endothelial cells (ECs). We report here that OSS led to tyrosine phosphorylation and strong, continuous nuclear translocation of YAP in ECs that is dependent on integrin α5β1 activation. YAP overexpression in ECs blunted the anti-atheroprone effect of an integrin α5β1–blocking peptide (ATN161) in *Apoe*$^{-/-}$ mice. Activation of integrin α5β1 induced tyrosine, but not serine, phosphorylation of YAP in ECs. Blockage of integrin α5β1 with ATN161 abolished the phosphorylation of YAP at Y^{357} induced by OSS. Mechanistic studies showed that c-Abl inhibitor attenuated the integrin α5β1–induced YAP tyrosine phosphorylation. Furthermore, the phosphorylation of c-Abl and YAP^{Y357} was significantly increased in ECs in atherosclerotic vessels of mice and in human plaques versus normal vessels. Finally, bosutinib, a tyrosine kinase inhibitor, markedly reduced the level of YAP^{Y357} and the development of atherosclerosis in *Apoe*$^{-/-}$ mice. The c-Abl/YAP^{Y357} pathway serves as a mechanism for the activation of integrin α5β1 and the atherogenic phenotype of ECs in response to OSS, and provides a potential therapeutic strategy for atherogenesis.

Introduction

Atherosclerosis has become one of the major causes of death worldwide because of its severe complications, such as acute myocardial infarction and stroke (1). Vascular endothelial cell (EC) activation is an initial step of atherosclerosis. ECs are responsive to various chemical and mechanical stimuli, including tumor necrosis factor α, lipopolysaccharide, and shear stress. EC activation triggers inflammatory responses to increase the expression of intercellular adhesion molecule 1 (ICAM-1) and vascular adhesion molecule 1 (VCAM-1), and the subsequent local recruitment of immune cells (2). As the interface between circulating blood and the vessel wall, ECs are constantly exposed to mechanical forces generated by blood flow. Atherosclerosis preferentially develops at branches and curvatures in the arterial tree where flow is disturbed. In contrast, the flow in straight parts of the arteries generates laminar shear stress (LSS), which is atheroprotective (3).

The Hippo pathway plays an evolutionarily conserved fundamental role in controlling organ size (4). The core components of the mammalian Hippo pathway contain kinase cascade of mammalian Ste20-like kinases 1/2 (Mst1/2) and large tumor suppressor 1/2 (Lats1/2). Mst1/2, in complex with a regulatory protein salvador (Sav1), phosphorylates and activates Lats1/2, which also forms a complex with a regulatory protein Mps-one-binding (Mob1) (5). The transcription coactivator Yes-associated protein (YAP) is a major downstream effector of the Hippo pathway (6). When the Hippo signaling pathway is inactivated, YAP and its paralog TAZ translocate into the nucleus and activate gene transcription by binding to the TEAD family and other transcription factors (4). The subcellular localization of YAP, which is important for its transcriptional activity, is regulated by its phosphorylation status. Phosphorylation at S^{127} of YAP leads to its direct binding to 14-3-3 and retention in cytoplasm (4, 7). Phosphorylation of YAP S^{397} (S^{381}) by Lats1/2 promotes YAP ubiquitination-dependent degradation and reduces its nuclear localization (8). In addition, phosphorylation of YAP at Y^{357} increases its stability and in turn upregulates its activity (9). Recently, YAP was identified to be crucial in ECs in different biological processes, including angiogenesis (10) and atherosclerosis (11, 12). Moreover, the suppression of YAP in response to LSS plays an important role in maintaining vessel homeostasis in ECs (11, 12). However, the regulation of YAP by OSS and the underlying mechanism is largely unknown.

Integrins, a diverse family of cell-surface heterodimeric proteins that facilitate cell–extracellular matrix (ECM) adhesion (13), are associated with endothelial activation (14–16). We and other groups identified integrin α5β1 as a membrane mechanical sensor responsive to OSS and with a proinflammatory and atheroprone role in ECs (17–19). Additionally, fibronectin, as an endogenous ligand that activates integrin α5β1 (20), can amplify the effect of oscillatory flow on EC activation (19). In contrast, an integrin α5 inhibitor peptide, ATN161, retards the development of atherosclerosis (17). However, the signal transduction underlying integrin activation remains unknown.

Nonreceptor protein tyrosine kinases (NRTKs), which transfer phosphate groups to tyrosine residues on protein substrates in the cytoplasm, are important components of signaling pathways

Authorship note: BL and JH contributed equally to this work.
Conflict of interest: The authors have declared that no conflict of interest exists.

Submitted: May 23, 2018; **Accepted:** January 3, 2019.
Reference information: *J Clin Invest*. 2019;129(3):1167–1179.
https://doi.org/10.1172/JCI122440.

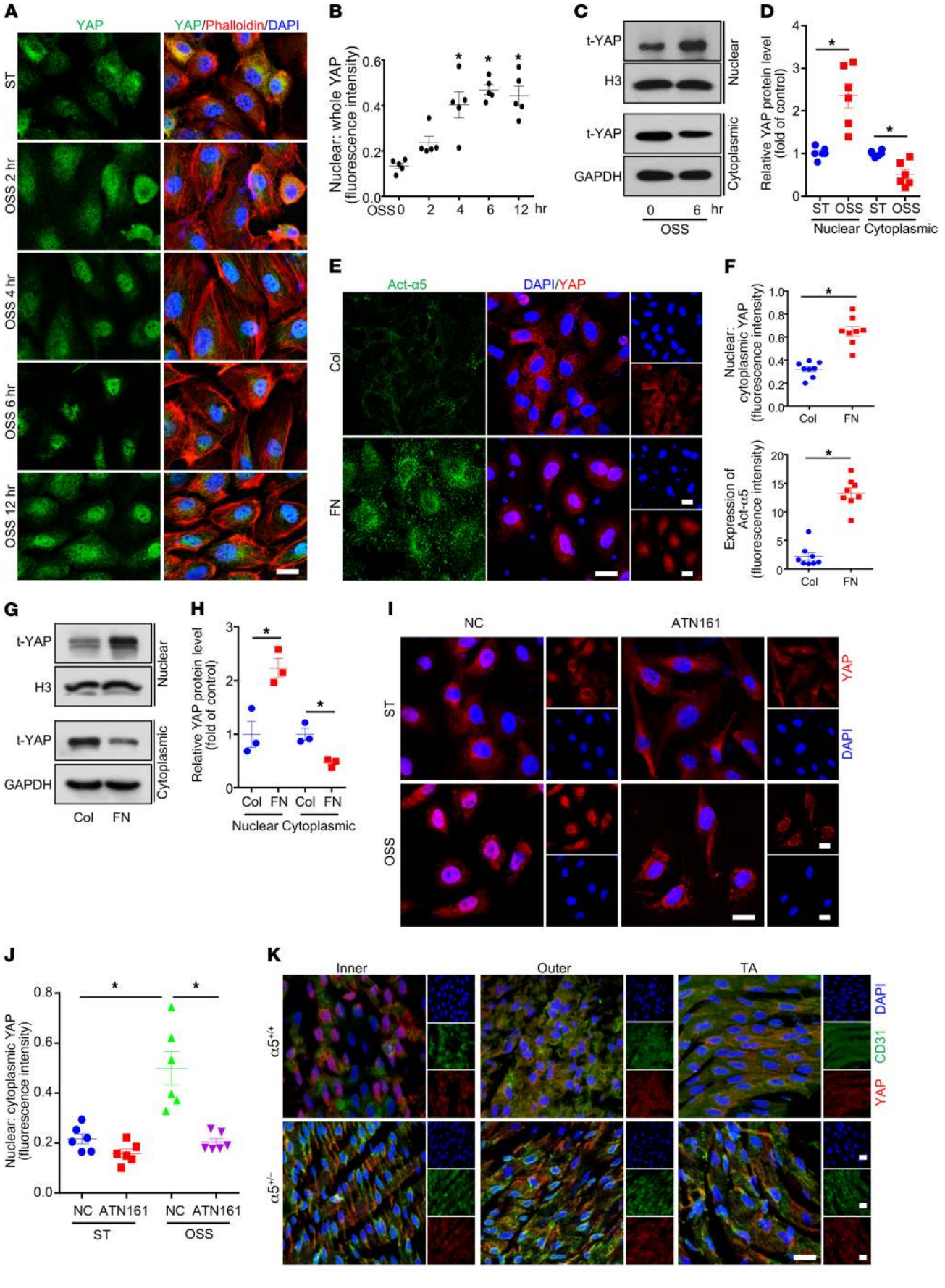
A
YAP
YAP/Phalloidin/DAPI
ST
OSS 2 hr
OSS 4 hr
OSS 6 hr
OSS 12 hr
B
Nuclear: whole YAP (fluorescence intensity)
OSS 0 2 4 6 12 hr
C
t-YAP
H3
Nuclear
t-YAP
GAPDH
Cytoplasmic
0 6 hr
OSS
D
Relative YAP protein level (fold of control)
ST OSS ST OSS
Nuclear Cytoplasmic
E
Act-α5
DAPI/YAP
Col
FN
F
Nuclear: cytoplasmic YAP (fluorescence intensity)
Col FN
Expression of Act-α5 (fluorescence intensity)
Col FN
G
t-YAP
H3
Nuclear
t-YAP
GAPDH
Cytoplasmic
Col FN
H
Relative YAP protein level (fold of control)
Col FN Col FN
Nuclear Cytoplasmic
I
NC
ATN161
ST
OSS
YAP
DAPI
J
Nuclear: cytoplasmic YAP (fluorescence intensity)
NC ATN161 NC ATN161
ST OSS
K
Inner
Outer
TA
α5+/+
α5+/−
DAPI
CD31
YAP

Figure 1. Oscillatory shear stress (OSS) increased Yes-associated protein (YAP) nuclear translocation via integrin α5β1. (**A** and **B**) Human umbilical vein endothelial cells (HUVECs) were exposed to OSS (0.5 ± 4 dyn/cm^2) for the indicated times. Cells with static treatment (ST) were a control. After treatment, cells underwent immunofluorescence staining with YAP (green), phalloidin (red), and DAPI (blue). Percentage of nuclear YAP was quantified. Scale bar: 20 μm. Data are mean ± SEM, *P < 0.05 versus ST (1-way ANOVA with Bonferroni multiple comparison post hoc test), n = 5. (**C** and **D**) HUVECs were exposed to OSS for 6 hours. Western blot analysis of YAP subcellular distribution in nucleus and cytoplasm. Data are mean ± SEM, *P < 0.05 (Student's t test), n = 6. (**E**–**H**) HUVECs were seeded in dishes coated with collagen (Col) or fibronectin (FN) (10 μg/ml) for 6 hours. (**E**) Immunofluorescence staining for YAP (red), Act-α5 (green), and DAPI (blue). Scale bars: 20 μm. (**F**) Ratio of nuclear to cytoplasmic fraction of YAP and fluorescent intensity of Act-α5 in panel E. Data are mean ± SEM, *P < 0.05 (Student's t test), n = 8. (**G**) Western blot analysis of nuclear and cytoplasmic protein to detect YAP expression. (**H**) Quantification of t-YAP in panel G. Data are mean ± SEM, *P < 0.05 (Student's t test), n = 3. (**I**) HUVECs were exposed to OSS or ST for 6 hours with or without pretreatment with ATN161 (10 μmol/l). Immunofluorescence staining for YAP (red) and DAPI (blue). Scale bars: 20 μm. (**J**) Ratio of nuclear to cytoplasmic fraction of YAP in panel I. Data are mean ± SEM, *P < 0.05 (2-way ANOVA with Bonferroni multiple comparison post hoc test), n = 6. (**K**) En face immunostaining of YAP (red), CD31 (green), and DAPI (blue) in the inner and outer curvature of the aortic arch (AA) and thoracic aorta (TA) from WT ($\alpha5^{+/+}$) and *Itga5*$^{+/-}$ ($\alpha5^{+/-}$) mice (8 weeks old, n = 5). Scale bars: 20 μm.

(21). NRTKs are divided into 9 main families according to their structures. Several kinases from different families, including focal adhesion kinase (FAK) and c-Src, mediate the signal transduction of integrins (22). c-Abl has been shown to be colocalized with integrin α5 and activated in cells subjected to fibronectin treatment (23) or fluid shear stress (24). Furthermore, with the emerging importance of NRTKs in neurodegenerative diseases, chronic myeloid leukemia, and carcinogenesis, tyrosine kinase inhibitors are being used in the clinic (21). Although a spleen tyrosine kinase inhibitor, fostamatinib, has been found to attenuate atherogenesis in mice (25), there is a paucity of information on the NRTKs as a potential target for treating atherosclerosis.

In this study, we investigated the regulation of YAP by OSS and the underlying mechanism in ECs. Our study provides both in vivo and in vitro evidence that activation of integrin α5β1 and its downstream kinase c-Abl mediates the OSS-induced YAP nuclear translocation via phosphorylating YAP at Y^{357}. In addition, we have demonstrated that inhibition of c-Abl blunts the OSS-induced EC activation and the development of early-stage atherosclerosis.

Results

OSS increased YAP nuclear translocation via integrin α5β1. YAP, as a novel mechanosensor (26), has been reported to promote EC activation in response to blood flow (12). To investigate the effects of OSS on the pattern of YAP nuclear localization, human umbilical vein ECs (HUVECs) were subjected to OSS (0.5 ± 4 dyn/cm^2, 1 Hz) for different durations. YAP showed significant nuclear localization beginning from 4 hours and sustained until 12 hours, as compared with static treatment (Figure 1, A and B). Western blot analysis further confirmed the increased nuclear localization of YAP at 6 hours after OSS stimulation (Figure 1, C and D). Given that integrin α5β1 has been previously reported to mediate OSS-induced EC activation (17), and fibronectin is a major endogenous ligand of integrin α5β1 (22), we detected YAP nuclear translocation in ECs seeded on fibronectin-coated plates. As shown in Figure 1, E and F, both integrin α5β1 activation and YAP nuclear translocation were induced by fibronectin, as evidenced by immunofluorescent staining. Western blot analysis also indicated that YAP nuclear translocation was increased with fibronectin treatment (Figure 1, G and H).

To further test whether the regulation of YAP in response to OSS depends on integrin α5β1, we used ATN161, an integrin α5β1–blocking peptide, in OSS-treated ECs. Pretreatment with ATN161 did not alter the YAP subcellular localization in HUVECs under static conditions, but completely blocked the OSS-induced YAP nuclear translocation (Figure 1, I and J). Moreover, in vivo evidence was obtained by examining the subcellular distribution of YAP in aortas of WT and *Itga5* heterozygous knockout ($\alpha5^{+/-}$) mice. As shown in Figure 1K, YAP exhibited nuclear localization in the inner curvature of the aortic arch (AA) but not the outer curvature of the AA or the thoracic aorta (TA) of WT mice. The flow pattern–dependent difference of YAP cellular distribution was abated in $\alpha5^{+/-}$ mice (Figure 1K). Thus, integrin α5β1 is essential in flow-induced YAP subcellular localization in vivo.

EC-specific YAP overexpression blunts the atheroprotective effect of integrin α5β1 blockage. Next, we asked whether YAP overexpression could abolish the beneficial effects of integrin α5β1 inhibition in vivo. To answer this question, we crossbred loxp-stop-loxp *YAP*-transgenic mice with *Tie2-Cre* mice to generate *Tie2-Cre*$^{+/-}$*YAP*$^{flox/-}$ mice (EC-*YAP*^{tg}), and generated EC-specific *YAP*-overexpression mice on an *Apoe*$^{-/-}$ background (EC-*YAP*^{tg}*Apoe*$^{-/-}$). We treated those mice with or without an integrin-blocking peptide ATN161. After 4 weeks of the Western-type diet (WTD), Oil Red O staining of aortas revealed that, in comparison with the scramble peptide, ATN161 significantly decreased the total atherosclerotic area in aortas of *YAP*^{flox}*Apoe*$^{-/-}$ mice (Figure 2, A and B). Aortic root staining showed that ATN161 reduced the lesion area, lipid deposition, and macrophage infiltration, but had minimal effects on collagen fiber or vascular smooth muscle cell content (Figure 2, C–E and Supplemental Figure 1, A–D; supplemental material available online with this article; https://doi.org/10.1172/JCI122440DS1). In contrast, the overexpression of YAP in ECs of mice aggravated atherosclerosis, as compared with *YAP*^{flox}*Apoe*$^{-/-}$ mice (Figure 2, A–E). ATN161 treatment failed to prevent the development of atherosclerosis in EC-*YAP*^{tg} *Apoe*$^{-/-}$ mice (Figure 2, A–E). The levels of plasma triglyceride and cholesterol and blood pressure did not change among the groups (Figure 2F and Supplemental Figure 1E). These results indicate that YAP is an important downstream effector of integrin α5β1 in EC activation.

OSS induced phosphorylation of YAP at Tyr357 through integrin α5β1. Because the cellular localization of YAP was regulated by its protein phosphorylation modification, we determined the levels of YAP phosphorylation at Ser127 (4), Ser397 (8), and Tyr357 (9) under OSS. OSS significantly increased the level of p-YAP^{Y357}, while decreasing that of p-YAP^{S127} without altering p-YAP^{S397} (Figure 3, A and B). Simultaneously, the OSS activation of integrin α5β1 showed a similar time dependency as the p-YAP^{Y357} (Figure 3, A and B). Fibronectin, as an agonist of integrin α5β1, dose-dependently upregulated the protein levels of both active-integrin α5β1 and

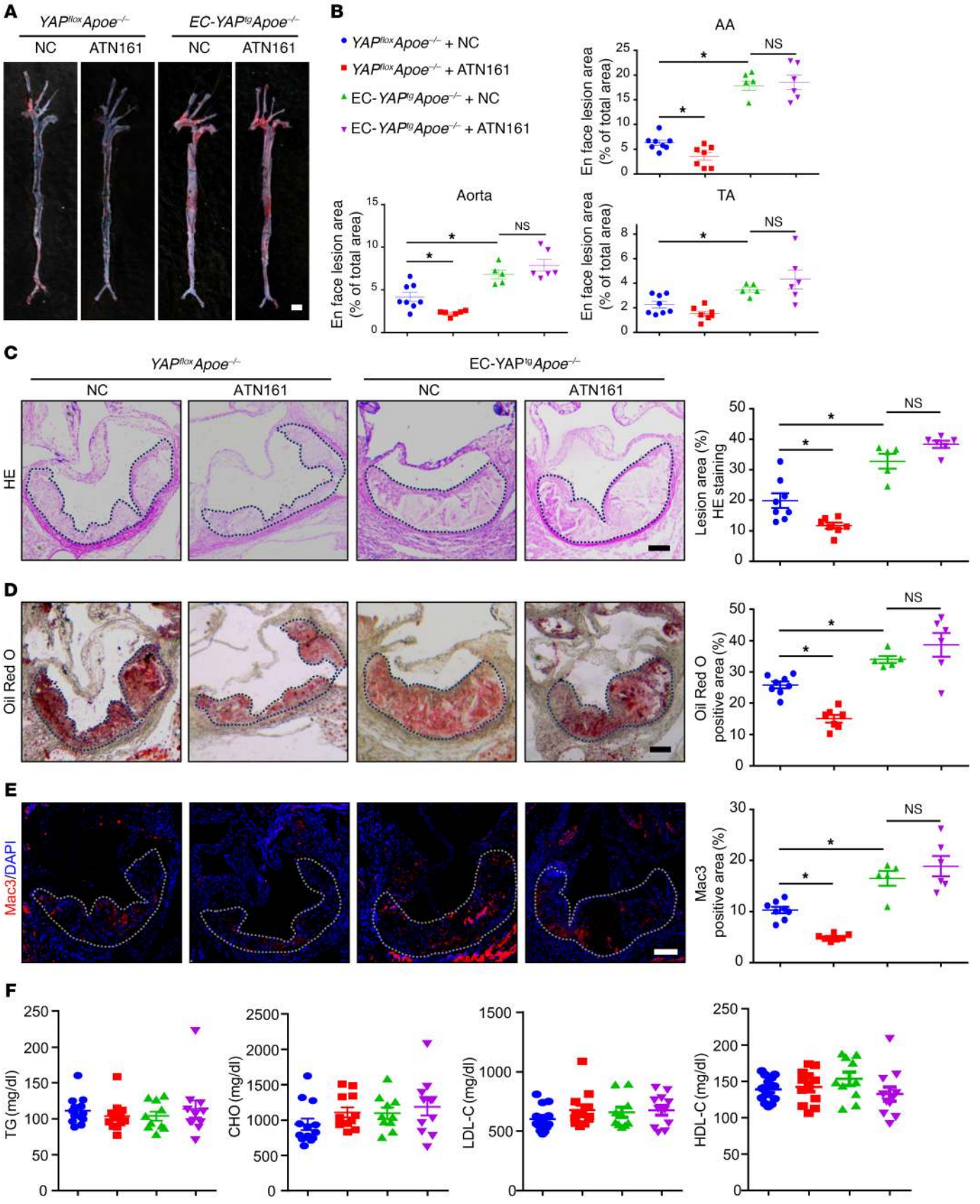
A
YAPflox Apoe−/−
EC-YAPtg Apoe−/−
NC
ATN161
NC
ATN161
B
YAPflox Apoe−/− + NC
YAPflox Apoe−/− + ATN161
EC-YAPtg Apoe−/− + NC
EC-YAPtg Apoe−/− + ATN161
AA
En face lesion area (% of total area)
Aorta
TA
NS
C
HE
Lesion area (%) HE staining
D
Oil Red O
Oil Red O positive area (%)
E
Mac3/DAPI
Mac3 positive area (%)
F
TG (mg/dl)
CHO (mg/dl)
LDL-C (mg/dl)
HDL-C (mg/dl)

Figure 2. EC specific *YAP* overexpression blunts the atheroprotective effect of integrin α5β1 blockage. EC-*YAP*^{tg}*Apoe*$^{-/-}$ and *YAP*^{flox}*Apoe*$^{-/-}$ mice were fed a WTD for 4 weeks, during which mice were intraperitoneally injected with scramble peptide (NC) or ATN161 (100 mg/kg) every 3 days. (**A**) Oil Red O staining of aortas. Scale bar: 4 mm. (**B**) Plaque area as a percentage of total area. AA, aortic arch; TA, thoracic aorta; NS, not significant. Data are mean ± SEM. *YAP*^{flox}*Apoe*$^{-/-}$ + NC (n = 8), *YAP*^{flox}*Apoe*$^{-/-}$ + ATN161 (n = 7), EC-*YAP*^{tg}*Apoe*$^{-/-}$ + NC (n = 5), EC-*YAP*^{tg}*Apoe*$^{-/-}$ + ATN161 (n = 6). *P < 0.05 (2-way ANOVA with Bonferroni multiple comparison post hoc test). (**C**–**E**) HE, Oil Red O, and Mac3 immunofluorescence staining of aortic roots. White dashed line indicates the size of plaque. Quantification of plaque size, Oil Red O–positive area in plaque and Mac3-positive area. Data are mean ± SEM. *YAP*^{flox}*Apoe*$^{-/-}$ + NC (n = 8), *YAP*^{flox}*Apoe*$^{-/-}$ + ATN161 (n = 7), EC-*YAP*^{tg}*Apoe*$^{-/-}$ + NC (n = 5), EC-*YAP*^{tg}*Apoe*$^{-/-}$ + ATN161 (n = 6). *P < 0.05 (2-way ANOVA with Bonferroni multiple comparison post hoc test). NS, not significant. Scale bars: 100 μm. (**F**) Plasma levels of triglycerides (TG), total cholesterol (CHO), low-density lipoprotein cholesterol (LDL-C), and high-density lipoprotein cholesterol (HDL-C). Data are mean ± SEM. *YAP*^{flox}*Apoe*$^{-/-}$ + NC (n = 13), *YAP*^{flox}*Apoe*$^{-/-}$ + ATN161 (n = 12), EC-*YAP*^{tg}*Apoe*$^{-/-}$ + NC (n = 10), EC-*YAP*^{tg}*Apoe*$^{-/-}$ + ATN161 (n = 11).

p-YAP^{Y357} (Figure 3, C and D). Meanwhile, fibronectin had little effect on the phosphorylation of YAP at Ser127 or Ser397 (Figure 3, C and D). In contrast, blockage of integrin α5β1 with ATN161 markedly decreased the OSS-induced protein levels of active integrin α5β1 and p-YAP^{Y357}, as well as the inflammatory markers (ICAM-1 and VCAM-1) (Figure 3, E and F). These results indicate that the OSS-induced EC proinflammatory phenotype was attributable, at least in part, to the integrin α5β1-YAP^{Y357} pathway.

Tyr357 phosphorylation of YAP induced endothelial activation both in vitro and in vivo. To assess the functional importance of YAP phosphorylation at Y357, we constructed adenovirus for YAP with mutation of Tyr357 to a non–phospho mimetic variant (Ad-YAP^{Y357F}), and explored its function in vitro and in vivo. At first, HUVECs were infected with Ad-GFP, Ad-YAP, or Ad-YAP^{Y357F} and then applied with OSS. OSS-induced upregulation of VCAM-1 protein level, as well as the increased number of THP-1 cells adhering to HUVECs, were exacerbated by overexpression of WT YAP, but not by the loss-of-function mutant Ad-YAP^{Y357F} (Figure 4, A–D). In vivo, the overexpression of YAP^{Y357F} increased the expression of VCAM-1 to a much lesser extent compared with those with Ad-YAP infection in left carotid artery endothelium of *Apoe*$^{-/-}$ mice with partial ligation (Figure 4, E and F). Our data suggest that pY357 of YAP in ECs plays a detrimental role in OSS-induced EC activation and atherogenesis.

Src/c-Abl pathway participates in integrin α5β1–mediated YAP phosphorylation at Tyr357. We next explored which tyrosine kinase was involved in OSS-induced YAPY357 phosphorylation in ECs. Because FAK was reported to mediate fibronectin-induced integrin α5β1 activation in smooth muscle cells (27), we first treated ECs with the FAK inhibitor PF-573228 (28) with or without fibronectin. PF-573228, which blocked fibronectin-mediated FAK phosphorylation at Tyr397, had no effect on p-YAP^{Y357} or YAP localization (Supplemental Figure 2, A and C). Next, we treated ECs with the Src family inhibitor (SU6656) and c-Abl inhibitor (nilotinib). SU6656 decreased p-YAP^{Y357} by 19%, and nilotinib almost abolished the fibronectin-induced phosphorylation of YAP^{Y357} (Supplemental Figure 2B and Figure 5A). The dual inhibition of the c-Abl and Src families by the use of bosutinib led to the reduction of the fibronectin-induced p-YAP^{Y357} protein by 88% (Figure 5B). Consistent with these findings, immunofluorescence staining of YAP indicates that its fibronectin-induced nuclear localization was blocked by Src/c-Abl inhibitors (Figure 5C and Supplemental Figure 2C). In addition, nilotinib or bosutinib treatment did not affect the proliferation or apoptosis of ECs (Supplemental Figure 2, D–K). Moreover, bosutinib treatment or siRNA-mediated knockdown of *ABL1* decreased OSS-induced upregulation of p-YAP^{Y357} and VCAM-1 at protein level (Figure 5, D–G).

p-c-Abl^{Y412} and p-YAP^{Y357} were highly expressed in ECs of atheroprone regions in both mouse and human. We next determined the expression of p-c-Abl^{Y412} and p-YAP^{Y357} in atheroprone regions of *Apoe*$^{-/-}$ mouse aortas. In the inner curvature and bifurcation of the AA where the flow is disturbed, both p-c-Abl^{Y412} and p-YAP^{Y357} were expressed at higher levels in ECs. In contrast, in the TA, where the flow is laminar, both p-c-Abl^{Y412} and p-YAP^{Y357} exhibited weak colocalization with the EC marker (Figure 6, A and B). Furthermore, the protein levels of p-c-Abl^{Y412}, p-YAP^{Y357}, and the EC activation marker VCAM-1 were significantly increased in the AA intima tissue lysates than those of TA intima (Figure 6, C and D). Consistent with these results in mice, the expression of both p-c-Abl^{Y412} and p-YAP^{Y357} in ECs of human coronary arteries was high in plaques but not in normal vessels (Figure 6, E and F). Taken together, these findings indicate a predominant role of c-Abl in regulating YAP phosphorylation at Tyr357 to contribute to the development of flow-dependent atherosclerosis.

Bosutinib retarded both diet-induced and partial ligation–induced atherosclerosis in Apoe$^{-/-}$ *mice*. In light of our finding that tyrosine kinase–mediated YAP phosphorylation might contribute to an atheroprone phenotype in ECs, bosutinib was injected into *Apoe*$^{-/-}$ mice that were fed a WTD for 4 or 12 weeks. Bosutinib significantly reduced the lesion area in aortas (Figure 7A and Supplemental Figure 3A). Oil Red O staining of whole aortas indicated that the reduction mainly occurred in the AA, where the lesion area was greatly decreased (Figure 7, B–E and Supplemental Figure 3, B–E). Lesion area and lipid deposition in aortic roots were also reduced by bosutinib (Supplemental Figure 3, F–K and Supplemental Figure 4, A–F), in parallel with the reduced levels of both p-c-Abl^{Y412} and p-YAP^{Y357} (Supplemental Figure 3, L and M and Supplemental Figure 4, G and H). In addition, blood pressure in *Apoe*$^{-/-}$ mice was not affected by long-term bosutinib treatment (Supplemental Figure 3N). Next, we used *Apoe*$^{-/-}$ mice with partial ligation to further test the effect of bosutinib. Consistent with the diet-induced model, bosutinib significantly reduced the development of atherosclerosis (Figure 7F). En face immunofluorescence staining of ligated carotid arteries showed that the levels of EC inflammatory markers VCAM-1 and ICAM-1 were abolished by bosutinib administration (Figure 7, G and H). These results indicate the atheroprotective effect of bosutinib on both early and advanced atherosclerosis.

Discussion

YAP has been identified as a mechanosensor of hemodynamic stress that contributes to EC activation in early-stage atherosclerosis (11, 12). However, the transduction signaling pathway linking shear stress and YAP is still unknown. Here, we found that under OSS, YAP nuclear translocation was partly mediated by

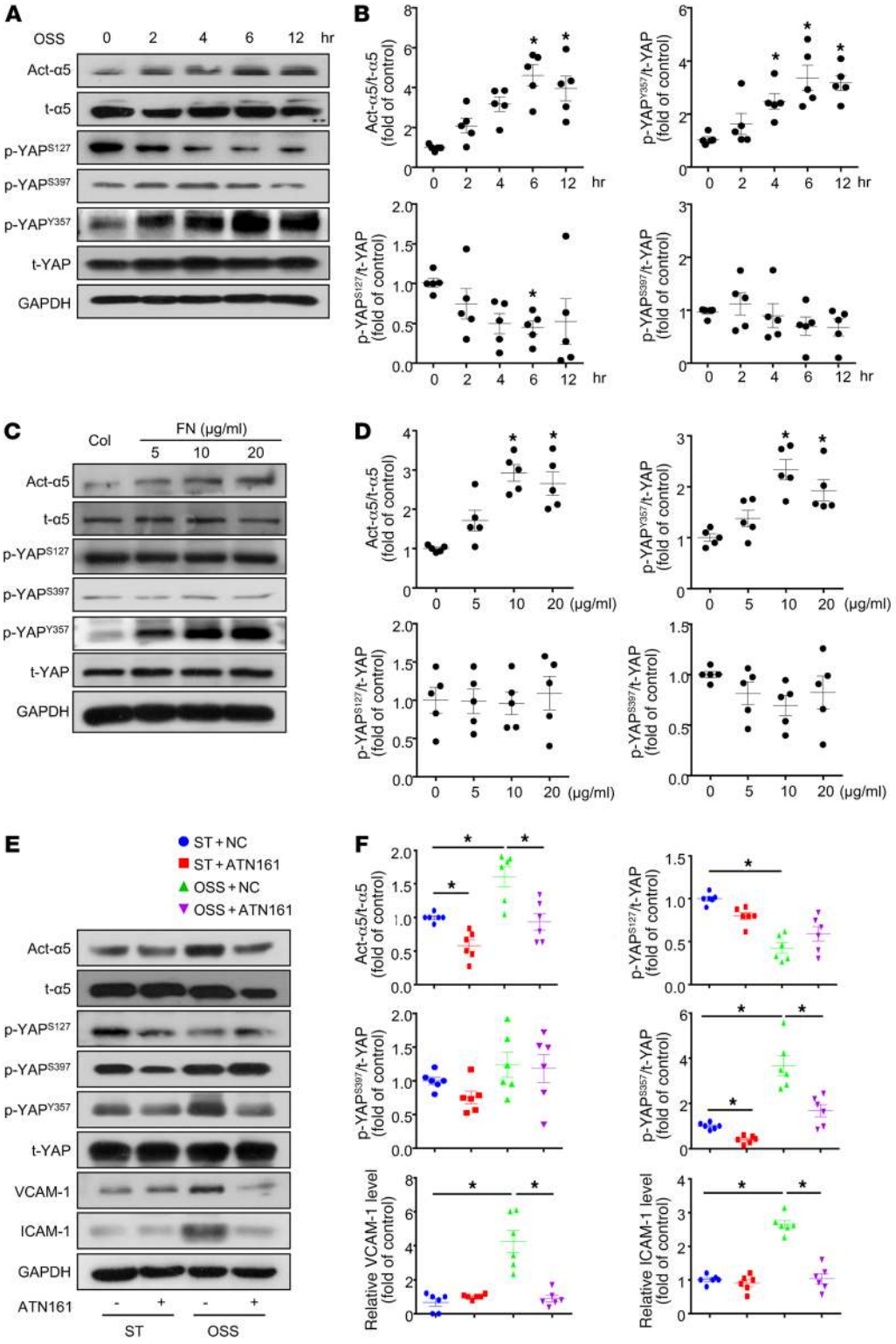

Figure 3. OSS induced phosphorylation of YAP at Tyr357 through integrin α5β1. (**A** and **B**) HUVECs were exposed to OSS for different times, as indicated. Cells with static treatment (ST) were a control. Western blot analysis of protein levels of activated integrin α5 (Act-α5), total integrin α5 (t-α5), p-YAP^{S127}, p-YAP^{S397}, p-YAP^{Y357} and t-YAP. (**B**) Quantification of YAP phosphorylation and Act-α5 normalized with t-YAP and t-α5. Data are mean ± SEM, $^*P < 0.05$ versus ST (1-way ANOVA with Bonferroni multiple comparison post hoc test), $n = 5$. (**C** and **D**) HUVECs were seeded on dishes coated with collagen (Col) or doses of fibronectin (FN) and cultured for 6 hours. Western blot analysis of protein level of activated integrin α5 (Act-α5), total integrin α5 (t-α5), p-YAP^{S127}, p-YAP^{S397}, p-YAP^{Y357}, and t-YAP. (**D**) Quantification of YAP phosphorylation and Act-α5 normalized to t-YAP and t-α5. Data are mean ± SEM, $^*P < 0.05$ (1-way ANOVA with Bonferroni multiple comparison post hoc test), $n = 5$. (**E**) HUVECs were exposed to OSS or ST for 6 hours with or without pretreatment of ATN161 (10 μmol/l). Western blot analysis of activated integrin α5 (Act-α5), integrin α5 (t-α5), p-YAP^{S127}, p-YAP^{S397}, p-YAP^{Y357}, t-YAP, ICAM-1, and VCAM-1. (**F**) Quantification of expressions of indicated proteins in panel E. Data are mean ± SEM, $^*P < 0.05$ (2-way ANOVA with Bonferroni multiple comparison post hoc test), $n = 6$.

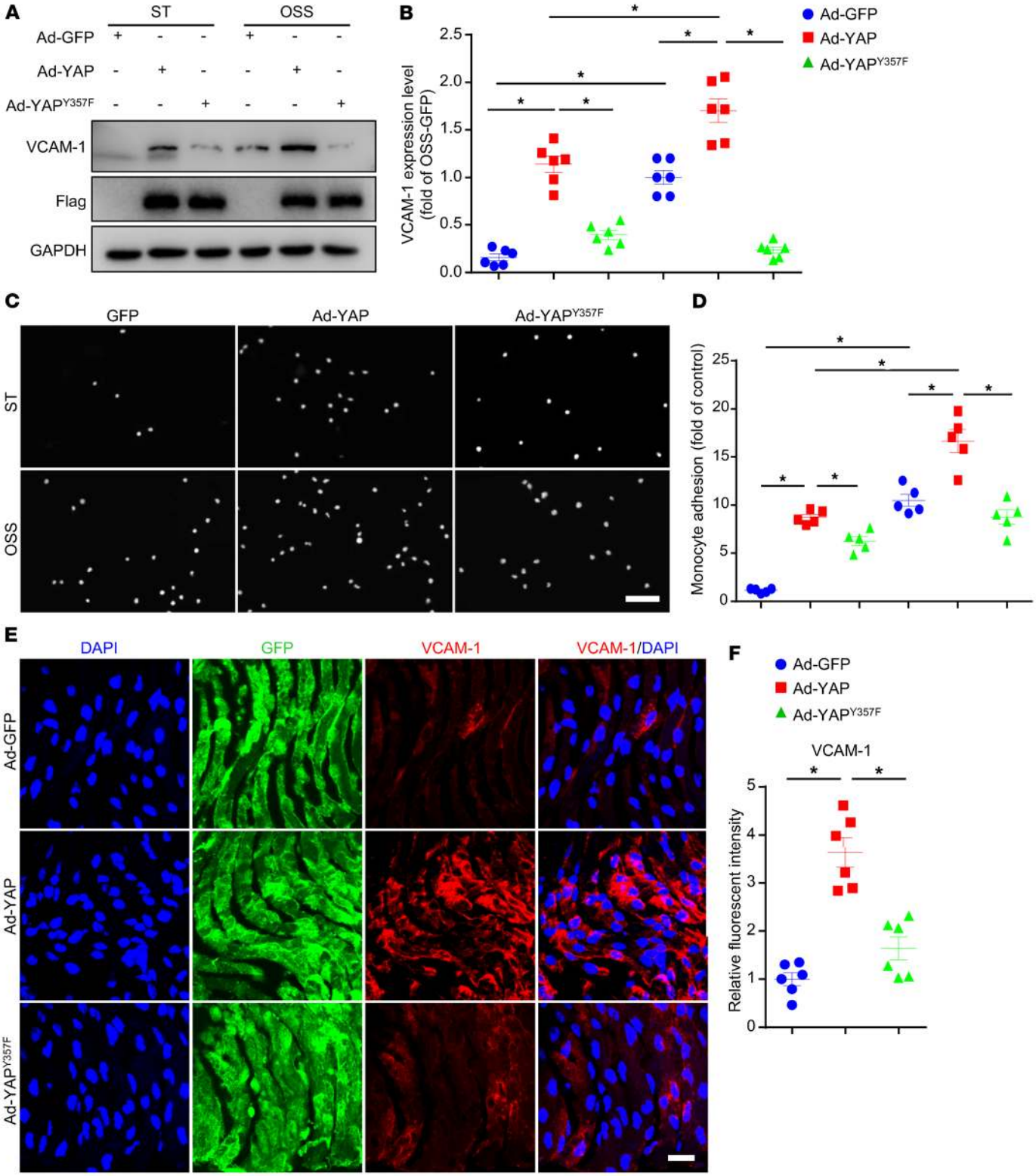

Figure 4. Tyr357 phosphorylation of YAP induced endothelial activation in vitro and in vivo. (**A** and **B**) HUVECs were infected with indicated adenoviruses for 24 hours with or without exposure to OSS or ST for another 6 hours. Western blot analysis of protein level of VCAM-1. Data are mean ± SEM, $^*P < 0.05$ (2-way ANOVA with Bonferroni multiple comparison post hoc test), $n = 6$. (**C** and **D**) HUVECs were infected with the indicated adenovirus for 24 hours with or without OSS. THP-1 cells were labeled with fluorescence dye, then cell adhesion assay was performed. Representative images of adhesive cells. Scale bar: 500 μm. Cell number from 5 random fields with ×10 objective was counted in each well. The number of adhesive cells was normalized to that of HUVECs with Ad-GFP infection. Data are mean ± SEM, $^*P < 0.05$ (2-way ANOVA with Bonferroni multiple comparison post hoc test), $n = 5$. (**E**) Male *Apoe*$^{-/-}$ mice underwent partial ligation of the carotid artery. During the ligation, carotid arteries were infused with the indicated adenovirus. Shows enface GFP and immunofluorescence staining of the expression of VCAM-1 in ECs of the carotid artery of mice. Scale bar: 20 μm. (**F**) Quantification of relative fluorescent intensity of VCAM-1. Data are mean ± SEM, $^*P < 0.05$ (Student's *t* test), $n = 6$ mice.

active integrin α5β1, which facilitates the activation of c-Abl and subsequent phosphorylation of YAP at Y^{357} in vivo and in vitro. As a ligand of integrin α5β1, fibronectin also increased the phosphorylation of YAP at Y^{357} via c-Abl. Use of a c-Abl inhibitor, bosutinib, greatly attenuated the development of both surgical partial ligation and dietary hypercholesterolemia-induced atherosclerosis in *Apoe*$^{-/-}$ mice.

Atherosclerotic plaques occur in a nonrandom manner and tend to develop in the vasculature locations with low shear stress and OSS. In addition, the deposited ECM also contributes to the preferential distribution of the atherosclerotic lesions, which is regulated by different flow patterns (29). For instance, the endothelium in atheroprotective regions resides on an ECM composed primarily of collagen IV and laminin (30), whereas fibronectin is preferentially deposited in atheroprone regions (31). Moreover, flow-induced tissue remodeling is highly dependent on ECM in atherosclerosis (32). pUR4, a fibronectin polymerization inhibitor, reduced the deposition of fibronectin in carotid arteries and significantly blocked flow-mediated accumulation of inflammatory cells and vascular remodeling (32). Besides the coupling of the external domain of integrins with the ECM to transduce signals into the cell, the conformational activation of integrin in responsive to ECMs is also induced by mechanical stimulation (33).

In this study, we found that the activation of integrin α5β1 in ECs involved specifically the phosphorylation of YAP^{Y357} under OSS, although OSS alters YAP phosphorylation at both Y^{357} and S^{127}. Consistent with this result, fibronectin increased YAP phosphorylation of only YAP^{Y357}, but not YAP^{S127}. These findings suggest that the activation of EC integrin α5β1 in response to atheroprone stimulations by both ECM fibronectin and OSS is dependent on YAP^{Y357}. Importantly, we demonstrated the relevance of YAP^{Y357} to the atheroprone regions in 2 rodent atherosclerosis models and human plaques. Because of the apparent redundancy of the integrins responsive to these stimuli (34), further experiments are needed to investigate the selective activation of integrins and their distinct downstream signaling pathways.

Tyrosine kinase is required to link the phosphorylation of YAP^{Y357} with the activation of integrin α5β1. Because of the structural diversity and varied catalytic domains of tyrosine kinases, the substrates of the tyrosine kinase family are distinguishable (35). According to previous reports, peptides with the motif YXXP are considered better substrates for c-Abl than other tyrosine kinases, and this is similar to the sequence surrounding Y357 (36). However, SU6656, a selective inhibitor for Src and other members of the Src family including Fyn and Yes (37), also partially blocked the fibronectin-induced YAP^{Y357} phosphorylation. This might be the result of the crosstalk between the c-Abl and Src families. c-Abl kinase activity could be upregulated by members of the Src family, and c-Abl can be directly phosphorylated by Fyn kinase (38). c-Abl also acts as a downstream effector of c-Src for growth factor–induced DNA synthesis (39). It is to be noted that c-Abl inhibitor (nilotinib) blocked integrin α5β1–induced YAP^{Y357} phosphorylation more markedly than did the Src inhibitor.

Given the interaction between these 2 pathways (37), we next used a dual Src/Abl kinase inhibitor and found that bosutinib profoundly reduced YAP^{Y357} phosphorylation. Moreover, OSS-induced YAP activation was attenuated by bosutinib. Bosutinib is a third-generation tyrosine kinase inhibitor of the Src/Abl pathway approved for adults with Philadelphia chromosome–positive chronic myeloid leukemia that is resistant and/or intolerant to prior therapy, and it has a more favorable hematologic toxicity profile than other tyrosine kinase inhibitors (40). Our results with animal models showed that bosutinib significantly reduced the lesion area in both diet- and ligation-induced atherosclerosis. Of note, bosutinib almost completely inhibited lesion formation in the AA but not TA in *Apoe*$^{-/-}$ mice; this strongly indicates that bosutinib attenuated the OSS-induced atheroprone effect. Hence, bosutinib may be a potential therapeutical agent for atherosclerotic diseases.

In conclusion, we found that the phosphorylation of YAP at Y357 and the consequent YAP activation in ECs are highly relevant in mouse and human atherosclerosis. OSS- or fibronectin-mediated activation of integrin α5β1 and c-Abl serves as an important upstream signal to facilitate the phosphorylation of YAP at Y357 (Figure 7I). Our findings reveal a novel YAP activation mechanism and provide evidence that the integrin α5β1/c-Abl/YAP pathway is a potential therapeutic target for early-stage atherosclerosis.

Methods

Antibodies and reagents. Antibodies against p-YAP^{Y357} (ab62751), t-YAP (ab52771), c-Abl (ab15130), p-c-Abl^{Y412} (ab47315), integrin α5 (ab150361), activated integrin α5 (ab72663), vWF (ab6994, ab11713), and CD31 (ab24590, ab28364) were from Abcam; t-YAP (catalog 14074), p-YAP^{S127} (catalog 4911), p-YAP^{S397}(catalog 13619), VCAM-1 (catalog 39036 for IF), Ki67 (catalog 11882) and dylight 594 phalloidin (catalog 12877) were from Cell Signaling Technology; and ICAM-1 (sc-7891), SMA (sc-53142), Mac3 (sc-20004), and VCAM-1 (sc-8304) (for Western blot analysis) were from Santa Cruz Biotechnology. Activated integrin α5 for IF (MABT201) was from Merck. The in situ cell death detection kit, anti-rabbit and anti-mouse secondary antibodies, and fibronectin were from Sigma-Aldrich. Imatinib, nilotinib, and bosutinib were from Selleckchem. The integrin α5 inhibitor ATN161 (Ac-PHSCN-NH2) and scramble peptide (Ac-HSPNC-NH2) were synthesized with 98% peptide purity by ChinaPeptides.

Cell culture and shear stress experiments. Human umbilical vein endothelial cells (HUVECs) were isolated and cultured as described (17, 41). For flow experiments, confluent monolayers of HUVECs were seeded on glass slides, and a parallel plate flow system was used to impose oscillatory flow (0.5 ± 4 dyn/cm^2). THP-1 cells (ATCC, catalog TIB-202) were cultured with 1640 medium supplemented with 10% fetal bovine serum. The flow system was enclosed in a chamber held at 37°C and ventilated with 95% humidified air plus 5% CO_2.

YAP recombinant adenovirus construction. Adenovirus expressing green fluorescent protein (Ad-GFP) and Ad-Flag-tagged human YAP (NM_001282101, Ad-YAP) were from GeneChem, as previously reported (10). Ad-YAP^{Y357F} was constructed using site-directed mutagenesis (GeneChem). HUVECs were infected with adenovirus at a multiplicity of infection (MOI) of 10, and no detectable cellular toxicity was observed.

Western blot analysis. Cells or tissues were homogenized in cold RIPA lysis buffer supplemented with complete protease inhibitor cocktail and phosSTOP phosphatase inhibitor (Roche). Protein was resolved by SDS-PAGE and transferred to PVDF membrane (Bio-Rad). Target protein was detected by using a specific primary antibody

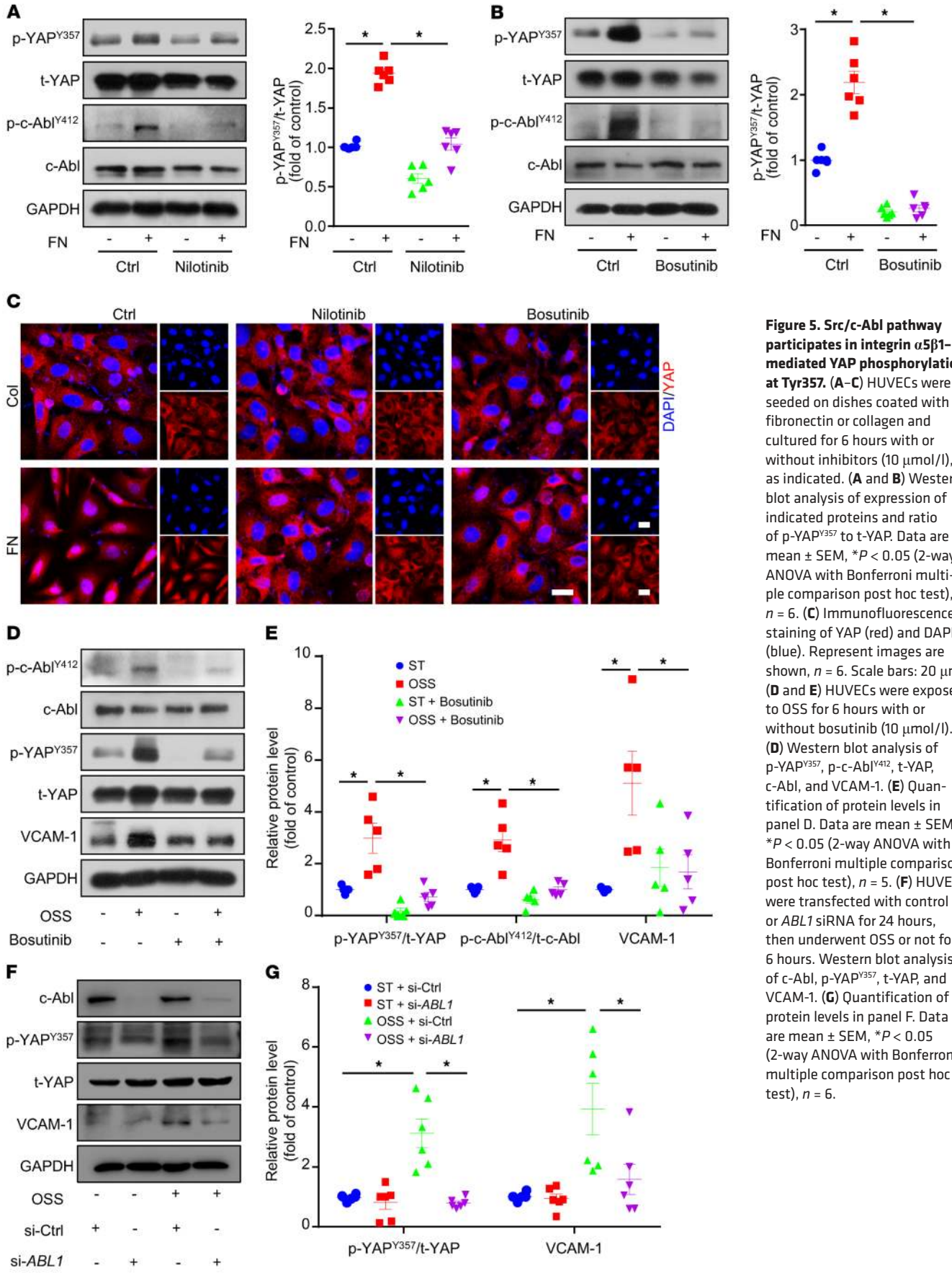

Figure 5. Src/c-Abl pathway participates in integrin α5β1–mediated YAP phosphorylation at Tyr357. (**A**–**C**) HUVECs were seeded on dishes coated with fibronectin or collagen and cultured for 6 hours with or without inhibitors (10 μmol/l), as indicated. (**A** and **B**) Western blot analysis of expression of indicated proteins and ratio of p-YAP^{Y357} to t-YAP. Data are mean ± SEM, $^*P < 0.05$ (2-way ANOVA with Bonferroni multiple comparison post hoc test), $n = 6$. (**C**) Immunofluorescence staining of YAP (red) and DAPI (blue). Represent images are shown, $n = 6$. Scale bars: 20 μm. (**D** and **E**) HUVECs were exposed to OSS for 6 hours with or without bosutinib (10 μmol/l). (**D**) Western blot analysis of p-YAP^{Y357}, p-c-Abl^{Y412}, t-YAP, c-Abl, and VCAM-1. (**E**) Quantification of protein levels in panel D. Data are mean ± SEM, $^*P < 0.05$ (2-way ANOVA with Bonferroni multiple comparison post hoc test), $n = 5$. (**F**) HUVECs were transfected with control or *ABL1* siRNA for 24 hours, then underwent OSS or not for 6 hours. Western blot analysis of c-Abl, p-YAP^{Y357}, t-YAP, and VCAM-1. (**G**) Quantification of protein levels in panel F. Data are mean ± SEM, $^*P < 0.05$ (2-way ANOVA with Bonferroni multiple comparison post hoc test), $n = 6$.

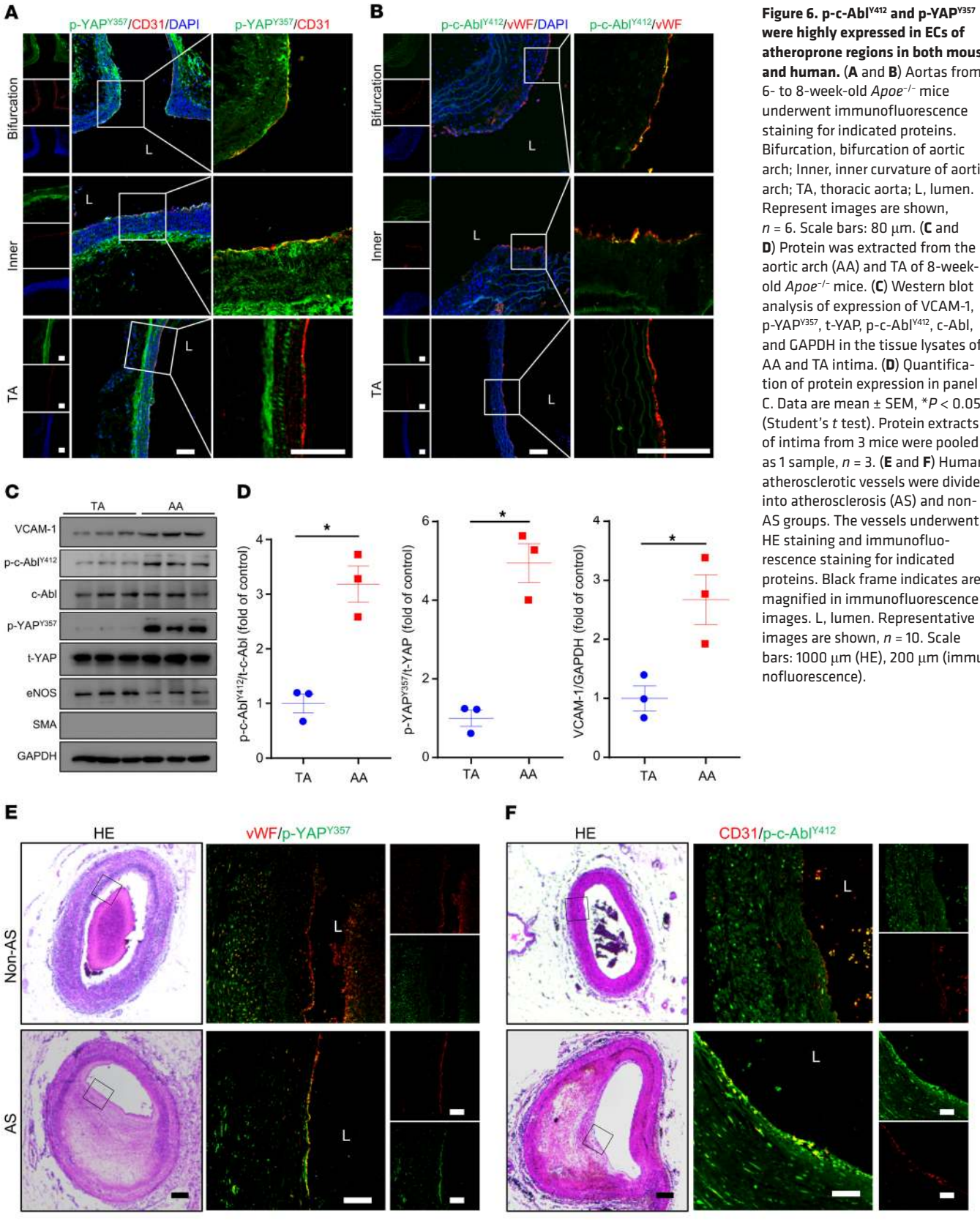

Figure 6. p-c-Abl^{Y412} and p-YAP^{Y357} were highly expressed in ECs of atheroprone regions in both mouse and human. (**A** and **B**) Aortas from 6- to 8-week-old *Apoe*$^{-/-}$ mice underwent immunofluorescence staining for indicated proteins. Bifurcation, bifurcation of aortic arch; Inner, inner curvature of aortic arch; TA, thoracic aorta; L, lumen. Represent images are shown, $n = 6$. Scale bars: 80 μm. (**C** and **D**) Protein was extracted from the aortic arch (AA) and TA of 8-week-old *Apoe*$^{-/-}$ mice. (**C**) Western blot analysis of expression of VCAM-1, p-YAP^{Y357}, t-YAP, p-c-Abl^{Y412}, c-Abl, and GAPDH in the tissue lysates of AA and TA intima. (**D**) Quantification of protein expression in panel C. Data are mean ± SEM, $^*P < 0.05$ (Student's *t* test). Protein extracts of intima from 3 mice were pooled as 1 sample, $n = 3$. (**E** and **F**) Human atherosclerotic vessels were divided into atherosclerosis (AS) and non-AS groups. The vessels underwent HE staining and immunofluorescence staining for indicated proteins. Black frame indicates area magnified in immunofluorescence images. L, lumen. Representative images are shown, $n = 10$. Scale bars: 1000 μm (HE), 200 μm (immunofluorescence).

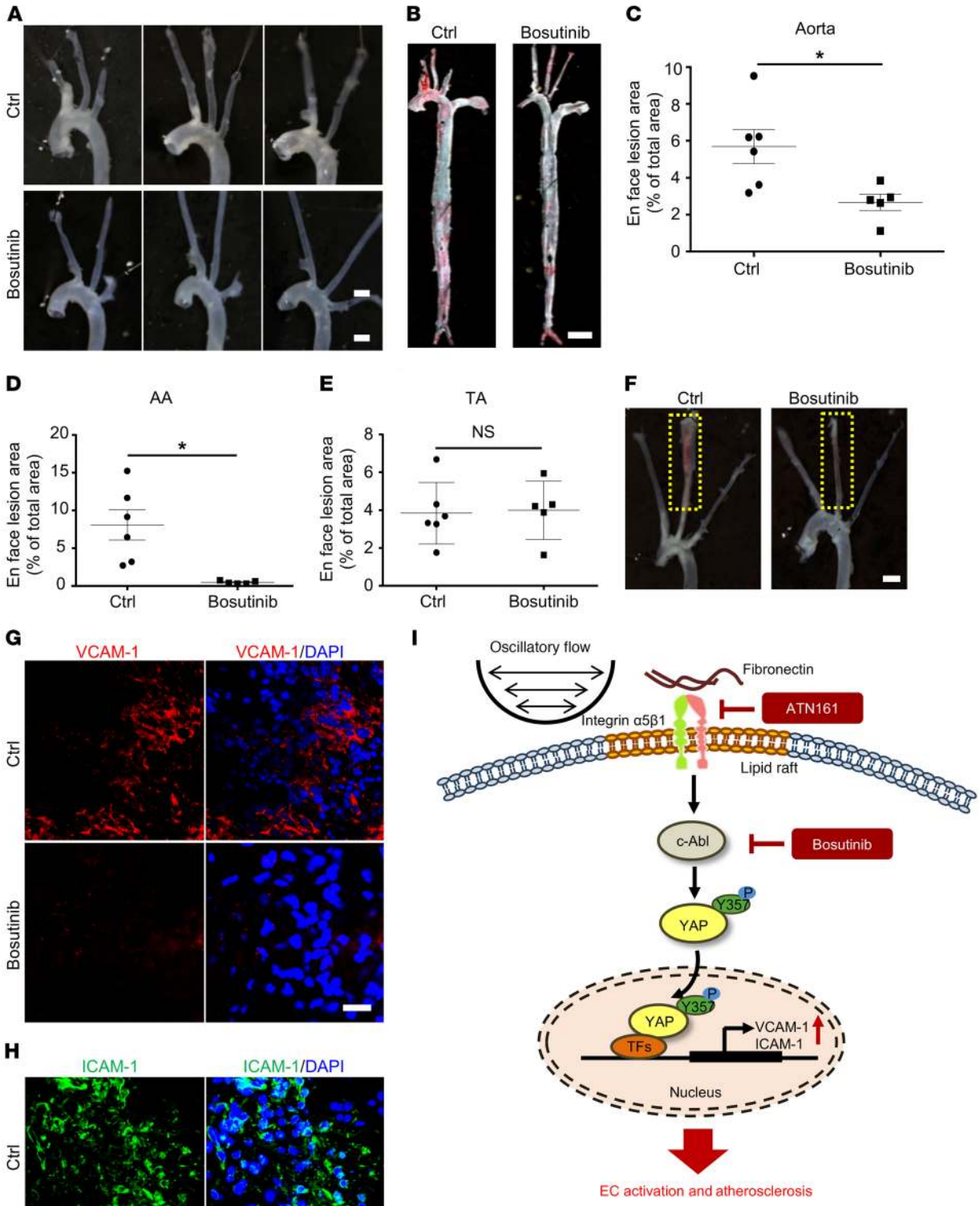

Figure 7. Bosutinib retarded both diet-induced and partial ligation–induced atherosclerosis in *Apoe*$^{-/-}$ mice. (**A**–**E**) Bosutinib (30 mg/kg) was injected every 3 days for 5 weeks into *Apoe*$^{-/-}$ mice, which were fed a WTD from the second week. (**A** and **B**) Representative gross and Oil Red O staining of aortas. Scale bar: 1.5 mm (**A**); Scale bar: 4 mm (**B**). (**C**–**E**) Quantification of lesion area in panel B. AA, aortic arch; TA, thoracic aorta; NS, not significant. Data are mean ± SEM, *$P < 0.05$ (Student's *t* test), $n = 5$–6. (**F**–**H**) Partial ligation was performed on left common carotid artery of *Apoe*$^{-/-}$ mice with or without bosutinib. Representative images are shown in panel F, $n = 6$. Scale bar: 2 mm (**F**). (**G** and **H**) En face immunofluorescence staining of the expression of VCAM-1 and ICAM-1 in ECs of mice with carotid artery ligation, $n = 6$. Scale bar, 20 μm. (**I**) A proposed model of c-Abl/YAP regulated by oscillatory flow in EC activation and atherosclerosis.

(1:1000). Bound antibodies were detected by horseradish peroxidase–conjugated secondary antibody (1:5000) and visualized by enhanced chemiluminescence (Cell Signaling Technology).

Cell adhesion assay. THP-1 cells were labeled with CellTrace calcein red-orange AM (Thermo Fisher Scientific, catalog C34851), then plated onto HUVEC plates at 2×10^6 cells/well. After incubation for 60 minutes at 37°C, nonadherent cells were removed by washing 3 times with PBS. The numbers of stained adhering cells in 5 random fields were counted for each group under a fluorescence microscope.

Immunofluorescence staining. HUVECs, aortic root, or aorta sections were fixed with 4% paraformaldehyde for 15 minutes. After permeabilization/blocking in 0.05% Triton X-100 (in PBS) and 1% BSA for 30 minutes at room temperature, aortas were incubated at 4°C overnight in incubation buffer containing 1% BSA and primary antibodies (1:100) Mac3, α-SMA, activated-integrin α5, YAP1, vWF, p-YAP^{Y357}, p-c-Abl^{Y412}, VCAM-1, ICAM-1, and CD31. After being washed 3 times in PBS, aortas were incubated with Alexa Fluor 488– or Alexa Fluor 594–conjugated secondary antibodies (1:200, Thermo Fisher Scientific) for 1 hour at room temperature. Fluorescent signals were detected using Leica confocal laser scanning microscopy.

Animal experiments. The 6-week-old male *Apoe*$^{-/-}$ mice (catalog 002052) were purchased from the Jackson Laboratory. *Itga5*$^{+/-}$ mice and EC-*YAP*^{tg} mice were generated as previously reported (12, 17). Briefly, we crossbred loxp-stop-loxp *YAP*-transgenic mice with *Tie2-Cre* mice to generate *Tie2-Cre*–mediated *YAP* transgenic mice (EC-*YAP*^{tg}). All EC-*YAP*^{tg} and *Itga5*$^{+/-}$ mice were bred in a C57BL/6 background. ATN161, scramble peptide, bosutinib, or dimethyl sulfoxide was intraperitoneally injected every 3 days for 5 or 13 weeks, and then mice were fed a WTD (Research Diets, catalog D12109C) containing 40 kcal% fat, 1.25% cholesterol, and 0.5% cholic acid for 4 or 12 weeks from the second week.

Partial ligation of the carotid artery was performed as described (17). *Apoe*$^{-/-}$ mice were anesthetized by using isoflurane (2%–3%). The left carotid artery was exposed by creating a ventral midline incision (4 mm–5 mm) in the neck. The left external carotid, internal carotid, and occipital arteries were ligated; the superior thyroid artery was left intact. Mice were monitored until recovery in a chamber on a heating pad after surgery. For bosutinib administration studies, bosutinib or dimethyl sulfoxide was intraperitoneally injected every 3 days for 3 weeks. Surgery was performed at the end of first week, and then mice were fed WTD for the last 2 weeks. For adenovirus infection studies, a single exposure of 5×10^8 plaque-forming units of adenovirus was luminally delivered to the left carotid artery and kept inside for 40 minutes to allow for sufficient infection. The adenovirus solution was subsequently removed and blood flow was restored. Mice were fed WTD immediately after the surgery for 1 week. Blood pressure of mice was monitored by a tail-cuff system (Softron, BP-98A). Each blood pressure value was averaged from 3 consecutive measurements per mouse.

Quantification of lipid levels. Blood samples were collected by tail bleeding into heparin-coated tubes. Plasma was separated by centrifugation. Total plasma cholesterol (CHO), triglycerides (TGs), low density lipoprotein cholesterol (LDL-C), and high-density lipoprotein cholesterol (HDL-C) levels were measured using kits from BioSino Bio-Technology and Science.

Human samples and staining. Human coronary arteries were obtained as we previously reported (42). Briefly, coronary arteries with or without atherosclerotic plaque were collected from the Verification Centre of Forensic Medicine affiliated with Shantou University. Immunofluorescence and HE staining were performed.

Statistics. Sample sizes were designed with adequate power according to the literature and our previous studies. No sample outliers were excluded. The experiments were not randomized and the investigators were not blinded to allocation during experiments and outcome assessment. The variance between the groups that were being statistically compared was similar. Data are mean ± SEM. Statistical analysis involved use of GraphPad Prism 6 by 2-tailed, unpaired Student's *t* test, and 1-way ANOVA or 2-way ANOVA with Bonferroni multiple comparison post hoc test, as appropriate. In all experiments, *P* less than 0.05 was considered statistically significant.

Study approval. Studies using autopsy tissue were approved by the Ethics Committee of Tianjin Medical University. Family members of subjects provided written informed consent for autopsy. The investigation conformed to the *Guide for the Care and Use of Laboratory Animals* (National Academies Press, 2011). All animal protocols were reviewed and approved by the Animal Care and Use Committee at Tianjin Medical University.

Author contributions

YZ and DA designed research; BL, JH, HL, YL, XL, and CZ performed research; BL and JH analyzed data; and BL, JH, YZ, and DA wrote the paper.

Acknowledgments

This work was supported by grants from the Ministry of Science and Technology of China (2017YFC1307402, 2016YFC0903000) and the National Natural Science Foundation of China (91849105, 81730014, 81420108003, 81670388, 81870313). YZ is a fellow in the Jiangsu Collaborative Innovation Center for Cardiovascular Disease Translational Medicine.

Address correspondence to: Yi Zhu or Ding Ai, Department of Physiology and Pathophysiology, Tianjin Medical University, 22 Qixiangtai Rd, Tianjin, China, 300070. Phone: 86.22.83336665; Email: zhuyi@tmu.edu.cn (YZ). Phone: 86.22.83336591; Email: edin2000cn@gmail.com (DA).

1. Desjardins F, Balligand JL. Nitric oxide-dependent endothelial function and cardiovascular disease. *Acta Clin Belg*. 2006;61(6):326–334.
2. Humphrey JD, Dufresne ER, Schwartz MA. Mechanotransduction and extracellular matrix homeostasis. *Nat Rev Mol Cell Biol*. 2014;15(12):802–812.
3. Davies PF. Hemodynamic shear stress and the endothelium in cardiovascular pathophysiology. *Nat Clin Pract Cardiovasc Med*. 2009;6(1):16–26.
4. Zhao B, et al. Inactivation of YAP oncoprotein by the Hippo pathway is involved in cell contact inhibition and tissue growth control. *Genes Dev*. 2007;21(21):2747–2761.
5. Zhao B, Li L, Lei Q, Guan KL. The Hippo-YAP pathway in organ size control and tumorigenesis: an updated version. *Genes Dev*. 2010;24(9):862–874.
6. Dong J, et al. Elucidation of a universal size-control mechanism in Drosophila and mammals. *Cell*. 2007;130(6):1120–1133.
7. Hao Y, Chun A, Cheung K, Rashidi B, Yang X. Tumor suppressor LATS1 is a negative regulator of oncogene YAP. *J Biol Chem*. 2008;283(9):5496–5509.

8. Zhao B, Li L, Tumaneng K, Wang CY, Guan KL. A coordinated phosphorylation by Lats and CK1 regulates YAP stability through SCF(beta-TRCP). *Genes Dev*. 2010;24(1):72–85.
9. Levy D, Adamovich Y, Reuven N, Shaul Y. Yap1 phosphorylation by c-Abl is a critical step in selective activation of proapoptotic genes in response to DNA damage. *Mol Cell*. 2008;29(3):350–361.
10. He J, et al. Yes-associated protein promotes angiogenesis via signal transducer and activator of transcription 3 in endothelial cells. *Circ Res*. 2018;122(4):591–605.
11. Wang KC, et al. Flow-dependent YAP/TAZ activities regulate endothelial phenotypes and atherosclerosis. *Proc Natl Acad Sci U S A*. 2016;113(41):11525–11530.
12. Wang l, et al. Integrin-YAP/TAZ-JNK cascade mediates atheroprotective effect of unidirectional shear flow. *Nature*. 2016;540(7634):579–582.
13. Jia J, et al. Dual inhibition of αV integrins and Src kinase activity as a combination therapy strategy for colorectal cancer. *Anticancer Drugs*. 2013;24(3):237–250.
14. Stupack DG, Cheresh DA. ECM remodeling regulates angiogenesis: endothelial integrins look for new ligands. *Sci STKE*. 2002;2002(119):pe7.
15. Short SM, Talbott GA, Juliano RL. Integrin-mediated signaling events in human endothelial cells. *Mol Biol Cell*. 1998;9(8):1969–1980.
16. Chen J, Green J, Yurdagul A, Albert P, McInnis MC, Orr AW. αvβ3 Integrins mediate flow-induced NF-κB activation, proinflammatory gene expression, and early atherogenic inflammation. *Am J Pathol*. 2015;185(9):2575–2589.
17. Sun X, et al. Activation of integrin α5 mediated by flow requires its translocation to membrane lipid rafts in vascular endothelial cells. *Proc Natl Acad Sci U S A*. 2016;113(3):769–774.
18. Yurdagul A, Green J, Albert P, McInnis MC, Mazar AP, Orr AW. α5β1 integrin signaling mediates oxidized low-density lipoprotein-induced inflammation and early atherosclerosis. *Arterioscler Thromb Vasc Biol*. 2014;34(7):1362–1373.
19. Yun S, et al. Interaction between integrin α5 and PDE4D regulates endothelial inflammatory signalling. *Nat Cell Biol*. 2016;18(10):1043–1053.
20. Hsia HC, Nair MR, Corbett SA. The fate of internalized α5 integrin is regulated by matrix-capable fibronectin. *J Surg Res*. 2014;191(2):268–279.
21. Gocek E, Moulas AN, Studzinski GP. Non-receptor protein tyrosine kinases signaling pathways in normal and cancer cells. *Crit Rev Clin Lab Sci*. 2014;51(3):125–137.
22. Schaffner F, Ray AM, Dontenwill M. Integrin α5β1, the Fibronectin Receptor, as a Pertinent Therapeutic Target in Solid Tumors. *Cancers (Basel)*. 2013;5(1):27–47.
23. Lewis JM, Baskaran R, Taagepera S, Schwartz MA, Wang JY. Integrin regulation of c-Abl tyrosine kinase activity and cytoplasmic-nuclear transport. *Proc Natl Acad Sci U S A*. 1996;93(26):15174–15179.
24. Tong H, et al. c-Abl tyrosine kinase regulates neutrophil crawling behavior under fluid shear stress via Rac/PAK/LIMK/cofilin signaling axis. *J Cell Biochem*. 2018;119(3):2806–2817.
25. Hilgendorf I, et al. The oral spleen tyrosine kinase inhibitor fostamatinib attenuates inflammation and atherogenesis in low-density lipoprotein receptor-deficient mice. *Arterioscler Thromb Vasc Biol*. 2011;31(9):1991–1999.
26. Dupont S, et al. Role of YAP/TAZ in mechanotransduction. *Nature*. 2011;474(7350):179–183.
27. Cai WJ, et al. Activation of the integrins alpha 5beta 1 and alpha v beta 3 and focal adhesion kinase (FAK) during arteriogenesis. *Mol Cell Biochem*. 2009;322(1-2):161–169.
28. Slack-Davis JK, et al. Cellular characterization of a novel focal adhesion kinase inhibitor. *J Biol Chem*. 2007;282(20):14845–14852.
29. Feaver RE, Gelfand BD, Wang C, Schwartz MA, Blackman BR. Atheroprone hemodynamics regulate fibronectin deposition to create positive feedback that sustains endothelial inflammation. *Circ Res*. 2010;106(11):1703–1711.
30. Sechler JL, Corbett SA, Wenk MB, Schwarzbauer JE. Modulation of cell-extracellular matrix interactions. *Ann N Y Acad Sci*. 1998;857:143–154.
31. Orr AW, Sanders JM, Bevard M, Coleman E, Sarembock IJ, Schwartz MA. The subendothelial extracellular matrix modulates NF-kappaB activation by flow: a potential role in atherosclerosis. *J Cell Biol*. 2005;169(1):191–202.
32. Chiang HY, Korshunov VA, Serour A, Shi F, Sottile J. Fibronectin is an important regulator of flow-induced vascular remodeling. *Arterioscler Thromb Vasc Biol*. 2009;29(7):1074–1079.
33. Batra N, et al. Mechanical stress-activated integrin α5β1 induces opening of connexin 43 hemichannels. *Proc Natl Acad Sci U S A*. 2012;109(9):3359–3364.
34. Kim C, Ye F, Ginsberg MH. Regulation of integrin activation. *Annu Rev Cell Dev Biol*. 2011;27:321–345.
35. Songyang Z, Cantley LC. Recognition and specificity in protein tyrosine kinase-mediated signalling. *Trends Biochem Sci*. 1995;20(11):470–475.
36. Songyang Z, et al. Catalytic specificity of protein-tyrosine kinases is critical for selective signalling. *Nature*. 1995;373(6514):536–539.
37. Blake RA, et al. SU6656, a selective src family kinase inhibitor, used to probe growth factor signaling. *Mol Cell Biol*. 2000;20(23):9018–9027.
38. Plattner R, Kadlec L, DeMali KA, Kazlauskas A, Pendergast AM. c-Abl is activated by growth factors and Src family kinases and has a role in the cellular response to PDGF. *Genes Dev*. 1999;13(18):2400–2411.
39. Furstoss O, Dorey K, Simon V, Barilà D, Superti-Furga G, Roche S. c-Abl is an effector of Src for growth factor-induced c-myc expression and DNA synthesis. *EMBO J*. 2002;21(4):514–524.
40. Cortes JE, et al. Bosutinib versus imatinib in newly diagnosed chronic-phase chronic myeloid leukemia: results from the BELA trial. *J Clin Oncol*. 2012;30(28):3486–3492.
41. Fu Y, et al. A novel mechanism of γ/δ T-lymphocyte and endothelial activation by shear stress: the role of ecto-ATP synthase β chain. *Circ Res*. 2011;108(4):410–417.
42. Wang Q, et al. Soluble epoxide hydrolase is involved in the development of atherosclerosis and arterial neointima formation by regulating smooth muscle cell migration. *Am J Physiol Heart Circ Physiol*. 2015;309(11):H1894–H1903.